

# Effect of support of Co-Na-Mo catalysts on the direct conversion of CO<sub>2</sub> to hydrocarbons

Rhodri E. Owen,<sup>a</sup> Pawel Plucinski,<sup>b</sup> Davide Mattia,<sup>b</sup> Laura Torrente-Murciano,<sup>c\*</sup> Valeska P. Ting<sup>b</sup> and Matthew D. Jones<sup>a\*</sup>

<sup>a</sup> Department of Chemistry, University of Bath, Claverton Down, Bath BA2 7AY, UK [mj205@bath.ac.uk](mailto:mj205@bath.ac.uk)

<sup>b</sup> Department of Chemical Engineering, University of Bath, Claverton Down, Bath BA2 7AY, UK

<sup>c</sup> Department of Chemical Engineering and Biotechnology, University of Cambridge, Cambridge CB2 3RA, UK. [lt416@cam.ac.uk](mailto:lt416@cam.ac.uk)

## Abstract

This study of the effect of support of Co-Na-Mo based catalysts on the direct hydrogenation of CO<sub>2</sub> into hydrocarbons (HC) provides guidelines for the design of catalysts for CO<sub>2</sub> conversion. We demonstrate that the surface area of the support and the metal-support interaction have a key role determining the cobalt crystallite size and consequently the activity of the system. Cobalt particles with sizes < 2 nm supported on MgO present low reverse water gas shift conversion with negligible Fischer-Tropsch activity. Increasing the cobalt particle size to ~ 15 nm supported on SiO<sub>2</sub> and ZSM-5 supports not only substantially increases the CO<sub>2</sub> conversion but it also provides high HC selectivities. Further increase of the cobalt particle size to 25-30 nm has a detrimental effect on the global CO<sub>2</sub> conversion with HC:CO ratios below 1, however, lower methane selectivity and enhanced formation of unsaturated HC products are achieved. Additionally, the metal-support interaction potentially also has a strong effect on the growth chain probability of the formed hydrocarbons, increasing as the metal-support interaction increases. These evidences demonstrate that CO<sub>2</sub> conversion and hydrocarbon distribution can be tuned towards desired products by controlled catalyst design.

## **Keywords**

Carbon Dioxide, Fischer-Tropsch, Cobalt, Support, Hydrocarbons.

## **1. Introduction**

Hydrocarbons, currently derived from crude oil, represent a vital source of fuel as well as an important feedstock for many industrial chemical processes. Despite the dependency of our lifestyle on this energy source, governments around the world, driven by environmental and social pressures, have recently agreed upon a global agreement for the decrease of CO<sub>2</sub> emissions associated to hydrocarbons derived from fossil fuels. While in the long term, a substitution of fossil fuels by renewable ones is desirable, the transition period is expected to be facilitated by an alternative, environmentally friendly production route of hydrocarbons.

One possibility for the production of carbon-containing chemicals, which is gaining increasing attention, is the capture of CO<sub>2</sub> and its conversion into hydrocarbons.<sup>1</sup> Atmospheric CO<sub>2</sub> levels are rising rapidly, recently passing the symbolic 400 ppm level and are set to continue to rise.<sup>2</sup> The increasing CO<sub>2</sub> concentration in the atmosphere is one of the largest contributing factors to global warming and as such, there is currently an increasing pressure on countries and industry to reduce CO<sub>2</sub> emissions. The possibility of considering CO<sub>2</sub> as a valuable chemical feedstock rather than a waste product is consequently becoming increasingly attractive as an exemplar of the circular economy.

A highly attractive route of CO<sub>2</sub> conversion is its two-step direct hydrogenation process consisting of the reduction of CO<sub>2</sub> to CO *via* the reverse water-gas shift (RWGS) reaction followed by the tandem conversion of the more reactive CO molecule into hydrocarbons through the Fischer-Tropsch (FT) process. The production of renewable hydrogen, as a way of storing excess

renewable energy from solar and wind sources, is currently attracting significant attention with many extremely promising technologies currently being developed,<sup>1b,3</sup>

Focusing on the conversion of CO<sub>2</sub>, one of the main challenges is associated with the development of catalysts not only with high activity but also with high selectivity to high value hydrocarbon products, specifically long chained hydrocarbons (C<sub>5+</sub>) and short chain olefins (C<sub>2</sub>-C<sub>4</sub>).<sup>1b,4</sup> Additionally, having both steps of the process occur simultaneously over a single catalyst under the same reaction conditions can reduce the cost and complexity of a large scale implementation of such technology.<sup>5</sup>

Most of the work to the date in this field has been focused on the use of conventional Fischer-Tropsch catalysts designed for CO-fed systems.<sup>6</sup> Iron-based systems have so far proved to be the most successful due to the RWGS activity of certain iron species which allows the formation of CO to be further converted into hydrocarbons.<sup>6</sup> On the other hand, cobalt-based catalysts are desirable for the production of heavier hydrocarbons in the industrial Fischer-Tropsch process due to their high activity, good selectivity and superior stability.<sup>7</sup> However, they normally present poor activity in the first CO<sub>2</sub> hydrogenation step.<sup>8</sup> Additionally, when CO<sub>2</sub> is added to a CO/H<sub>2</sub> stream, the hydrocarbon distribution is strongly affected with a shift in selectivity towards undesired products such as methane.<sup>5,9</sup> When the feed-gas is completely shifted to a CO<sub>2</sub>/H<sub>2</sub> mixture, cobalt systems tend to act as methanation catalysts with almost exclusively (generally >90 %) methane formed.<sup>5,10</sup>

To improve the catalyst performance, small concentrations of dopants are often added to both iron and cobalt based catalysts.<sup>11</sup> Promoters typically utilised with cobalt Fischer-Tropsch catalysts such as platinum and palladium have little effect on the product distribution when CO<sub>2</sub> is utilised as the carbon source.<sup>12</sup> Recent work conducted within our group has shown that addition

of molybdenum and sodium as promoters to cobalt enhances the selective production of C<sub>2+</sub> hydrocarbons.<sup>13</sup> Most of the work in the area is focused on the use of Al<sub>2</sub>O<sub>3</sub> supports, generally used in industrial Fischer Tropsch processes.<sup>14</sup> However, some studies have demonstrated that other inorganic oxide supports such as TiO<sub>2</sub> can outperform Al<sub>2</sub>O<sub>3</sub> in the Fischer Tropsch process using CO/H<sub>2</sub> feeds.<sup>14-15</sup> This work presents for the first time a systematic study of the effect of the support on Co-Na-Mo catalysts for the direct conversion of CO<sub>2</sub> into hydrocarbons, revealing the importance of the support not only on the cobalt crystallite size but also the key effect of the metal-support interaction on the hydrocarbon distribution.

## 2. Experimental

### 2.1 Catalyst Preparation

Cobalt – sodium – molybdenum catalysts were prepared by wet impregnation using Co(NO<sub>3</sub>)<sub>2</sub>·6H<sub>2</sub>O, NaOAc and (NH<sub>4</sub>)<sub>6</sub>Mo<sub>7</sub>O<sub>24</sub>·4H<sub>2</sub>O as metal precursors. A variety of supports were used including SiO<sub>2</sub> (Davisil, 35-70 μm particle size, 500 Å pore diameter), CeO<sub>2</sub> (Aldrich, powder < 5 μm), ZrO<sub>2</sub> (Aldrich, powder 5 μm), γ-Al<sub>2</sub>O<sub>3</sub> (Fluka), TiO<sub>2</sub> (Aldrich, Anatase), ZSM-5(NH<sub>4</sub><sup>+</sup>) (Alfa Aesar) and MgO (prepared by the calcination of Mg<sub>5</sub>(OH)<sub>2</sub>(CO<sub>3</sub>)<sub>4</sub>·xH<sub>2</sub>O†). In a typical synthesis, the support was suspended in the minimum amount of methanol. 20 mL of methanol containing 20 wt.% of cobalt was added drop-wise under stirring. Following this step, 1 wt.% of sodium dissolved in methanol and (NH<sub>4</sub>)<sub>6</sub>Mo<sub>7</sub>O<sub>24</sub>·4H<sub>2</sub>O dissolved in deionised water were added slowly into the solution. The resulting mixture was stirred for 10 minutes before being sonicated for 60 minutes. The solvent was removed under vacuum while being heated through the use of a rotary evaporator until a powder of constant mass was obtained. The obtained powder was then calcined in air for 16 hours at 873 K.

## 2.2 Catalyst Characterisation

Scanning electron microscopy characterisation was carried out on a JEOL 6480LV at 5 - 20 kV. Energy-dispersive X-ray spectroscopy (EDS) was carried out *in situ* during SEM analysis. X-ray diffraction studies were conducted on a BRUKER D8-Advanced diffractometer. Cu K $\alpha$  ( $\lambda = 1.5406 \text{ \AA}$ ) radiation was used for all samples (step size  $0.0164^\circ$  and 0.6 s per step). N<sub>2</sub> adsorption was carried out at 77 K after degassing (at 120 °C for 12 hrs under high vacuum) using a Micromeritics ASAP 2020 gas sorption analyser. Surface area values were calculated using the Brunauer-Emmett-Teller (BET) theory. Temperature programme reduction (TPR) experiments were carried out using a Micromeritics Autochem II instrument equipped with a thermal conductivity detector (TCD). Samples were reduced using 30 mL·min<sup>-1</sup> of 5% H<sub>2</sub>/Ar from room temperature up to 1000 °C with a ramp rate of 10 K·min<sup>-1</sup>.

## 2.3 Catalyst Testing

Catalysts were tested in a purpose built packed-bed reactor.† Typically, 1.0 g of catalyst was diluted with silicon carbide (Sigma Aldrich, 200-400  $\mu\text{m}$  particle size) and loaded into a stainless steel tube reactor (catalyst bed 150 mm length, 4.6 mm internal diameter). Prior to testing, the catalysts were reduced in-situ under a flow of pure hydrogen at 300 °C for 2 hours. Carbon dioxide hydrogenation reactions were conducted at atmospheric pressure and 200 °C with a H<sub>2</sub>:CO<sub>2</sub> ratio of 3:1 and a total flow of 8 sccm unless stated otherwise. Samples were taken from the exhaust gases of the reactor and analysed using an Agilent 7890A GC equipped with mass spectrometer as detector, this is further equipped with a TCD and FID detector. A 30m HP-PLOT/Q column was utilised for product analysis. The GC-MS was calibrated using a BOC special gas mixture

containing 1 % v/v CH<sub>4</sub>, C<sub>2</sub>H<sub>6</sub>, C<sub>3</sub>H<sub>6</sub>, C<sub>3</sub>H<sub>8</sub>, n-C<sub>4</sub>H<sub>10</sub>, CO, CO<sub>2</sub>, in N<sub>2</sub>. The mass balance was calculated based on the carbon content, being satisfied within  $\pm 5\%$ . Product selectivity was calculated on the carbon basis defined as moles of carbon in product  $x$ /moles of CO<sub>2</sub> converted. Multiple repeats of the catalytic data reproduced well with values of conversion and selectivity being within  $\pm 5\%$  of the values reported.

### 3. Results and Discussion

#### 3.1 Effect of support on CO<sub>2</sub> conversion and selectivity

In order to study the effect of the support of the activity of Co-Na-Mo-based catalysts on the direct conversion of CO<sub>2</sub> into hydrocarbons, a series of inorganic oxide supports were used namely SiO<sub>2</sub>, CeO<sub>2</sub>, TiO<sub>2</sub> Al<sub>2</sub>O<sub>3</sub>, MgO and ZrO<sub>2</sub> and ZSM-5(NH<sub>4</sub><sup>+</sup>). The catalysts were tested in a fixed bed reactor at atmospheric pressure at 200 °C using a H<sub>2</sub>:CO<sub>2</sub> ratio of 3:1. Table 1 shows the conversion, selectivity and hydrocarbon distribution.

**Table 1: Catalytic activity of 20wt.%Co-1wt.%Na-1wt.%Mo supported on a range of inorganic oxides.**

Entry	Catalyst Support	CO <sub>2</sub> Conversion /%	CO selectivity /%	HC selectivity /%	Hydrocarbon distribution							$\alpha$
					C <sub>1</sub>	C <sub>2=</sub>	C <sub>2</sub>	C <sub>3=</sub>	C <sub>3</sub>	C <sub>4</sub>	C <sub>5+</sub>	
1	SiO <sub>2</sub>	30.0	21.5	78.5	57.1	0.0	9.3	0.1	11.8	9.3	12.3	0.48
2	SiO <sub>2</sub> <sup>a</sup>	15.6	59.0	41.0	42.1	0.0	10.7	1.7	14.1	12.7	18.7	0.52
3	CeO <sub>2</sub>	15.1	70.2	29.8	22.1	0.92	12.8	9.8	9.1	14.1	31.2	0.59
4	TiO <sub>2</sub>	13.5	66.7	33.3	23.1	0.77	9.9	9.2	7.0	13.7	24.2	0.60
5	Al <sub>2</sub> O <sub>3</sub>	15.4	57.3	42.7	29.3	0.0	12.3	4.1	14.1	13.9	27.1	0.57
6	MgO	8.7	100	-	0.0	0.0	0.0	0.0	0.0	0.0	0.0	N.A.
7	ZrO <sub>2</sub>	14.4	16.7	83.3	26.8	0.0	14.8	12.9	8.2	14.9	22.4	0.52
8	ZSM-5	29.1	20.6	79.4	95.7	0.0	3.0	0.0	0.9	0.2	0.2	0.17

Reaction conditions 200 °C, 1 atm, 3:1 H<sub>2</sub>:CO<sub>2</sub> and 8 sccm total flow, WHSV: 0.35 h<sup>-1</sup>. <sup>a</sup> WHSV: 1.73 h<sup>-1</sup>.

The Co-Na-Mo catalysts supported on SiO<sub>2</sub> and ZSM-5 showed the highest CO<sub>2</sub> conversion

values, with similar CO and hydrocarbon selectivity. Catalysts supported on CeO<sub>2</sub>, TiO<sub>2</sub>, Al<sub>2</sub>O<sub>3</sub> and ZrO<sub>2</sub> present a similar CO<sub>2</sub> conversion under the studied conditions (~ 15%), however, the hydrocarbon selectivity versus CO decreases in the order of ZrO<sub>2</sub> < Al<sub>2</sub>O<sub>3</sub> < TiO<sub>2</sub> < CeO<sub>2</sub>. Finally, the catalyst showing the lowest conversion utilises MgO as the support, with no hydrocarbons being formed, with the sole presence of CO in the outlet stream.

The difference in CO<sub>2</sub> conversion can be partially explained based on the difference of cobalt crystallite size. Figure 1 shows the pXRD patterns of the different catalysts. In the Co-Na-Mo/SiO<sub>2</sub> catalysts, no diffraction peaks associated to the support are observed, confirming the amorphous nature of the silica. In contrast, diffraction peaks representative of CeO<sub>2</sub>, TiO<sub>2</sub> anatase,  $\gamma$ -Al<sub>2</sub>O<sub>3</sub>, MgO, ZrO<sub>2</sub> and ZSM-5 are observed for the corresponding catalysts.<sup>16</sup>

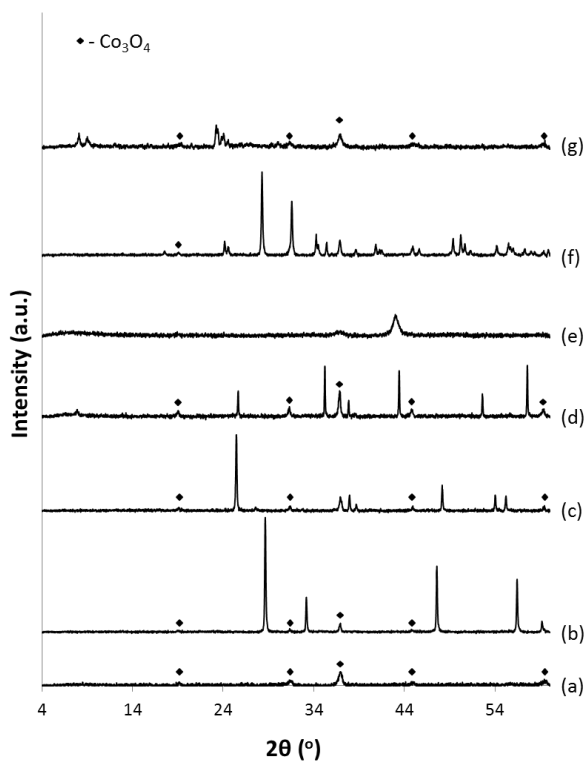


**Figure 1:** pXRD patterns of the 20 wt.%Co- 1 wt.%Na- 1 wt.%Mo catalysts supported on a. SiO<sub>2</sub>, b. CeO<sub>2</sub>, c. TiO<sub>2</sub>, d. Al<sub>2</sub>O<sub>3</sub>, e. MgO, f. ZrO<sub>2</sub> and g. ZSM-5. All peaks attributable solely to Co<sub>3</sub>O<sub>4</sub> are marked, while, any peaks overlapping with support peaks are not marked for clarity.

Additionally, the diffraction peaks at  $2\theta$  values of 19, 31, 37, 45 and 59 degrees, corresponding to the crystalline  $\text{Co}_3\text{O}_4$  phase<sup>17</sup> are observed in the  $\text{SiO}_2$ ,  $\text{CeO}_2$ ,  $\text{TiO}_2$ ,  $\text{Al}_2\text{O}_3$ ,  $\text{ZrO}_2$  and ZSM-5 supported catalysts. No peaks attributable to any other crystalline species are observed. Interestingly, no diffraction peaks corresponding to any of the crystalline cobalt phases were observed in the MgO supported system, suggesting the cobalt is highly dispersed or that the crystalline size is below the XRD detection limit ( $< 2$  nm). The average crystallite size of cobalt was calculated using the Scherrer equation, Table 2. The  $\text{Co}_3\text{O}_4$  phase supported on  $\text{SiO}_2$  and ZSM-5 present similar crystallite sizes (14 – 16 nm). The catalyst supported on  $\text{TiO}_2$  and  $\text{ZrO}_2$  present cobalt crystallite sizes  $\sim 22$ -24 nm, while larger cobalt crystallites (30 – 35 nm) are observed in the catalysts supported on  $\text{CeO}_2$  and  $\text{Al}_2\text{O}_3$ .

**Table 2: Surface area and  $\text{Co}_3\text{O}_4$  crystallite size of supported 20 wt.%Co- 1 wt.%Na- 1 wt.%Mo catalysts**

Catalyst Support	Surface Area / $\text{m}^2\text{g}^{-1}$	$\text{Co}_3\text{O}_4$ crystallite Size <sup>b</sup> / nm
$\text{SiO}_2$	56	15
$\text{CeO}_2$	7.0	34
$\text{TiO}_2$	14	23
$\text{Al}_2\text{O}_3$	6.1	30
MgO	54	-
$\text{ZrO}_2$	6.6	24
ZSM-5	180	15

<sup>a</sup> Estimated using the BET theory

<sup>b</sup>  $\text{Co}_3\text{O}_4$  particle size calculated from pXRD studies using the Scherrer equation.

The cobalt crystallite size seem to be, at least partially, related to the surface area of the support (Table 2). One should notice that the larger cobalt sizes are present in low surface area  $\text{CeO}_2$  and  $\text{Al}_2\text{O}_3$ , while higher cobalt dispersions are achieved in  $\text{SiO}_2$ , MgO and ZSM-5 with surface areas

above  $50 \text{ m}^2 \text{ g}^{-1}$ . However, interaction of the metals with the support has also been demonstrated to be critical for determining not only metal particle size but also their stabilisation against sintering.<sup>18</sup>

There seems to be a direct relationship between cobalt particle size and  $\text{CO}_2$  conversion. Cobalt particle sizes of  $\sim 15 \text{ nm}$  present in  $\text{SiO}_2$  and ZSM-5 show almost double  $\text{CO}_2$  conversion than those with particle sizes  $> 20 \text{ nm}$ . In this case, the  $\text{CO}_2$  conversion seems to be independent to the cobalt size within the  $20 - 35 \text{ nm}$  range. The cobalt particle size also appears to have an effect on the CO and hydrocarbon yield. As shown in Table 1, Co-Na-Mo supported on  $\text{SiO}_2$  and ZSM-5 present higher hydrocarbon selectivities. Larger cobalt particles size (supported on  $\text{CeO}_2$ ,  $\text{TiO}_2$ ,  $\text{Al}_2\text{O}_3$  and  $\text{ZrO}_2$ ) present a detrimental effect on the HC yield with HC/CO yield ratios below 1. On the other hand, very small cobalt crystallites ( $< 2 \text{ nm}$ ) supported on MgO produce CO only under the study conditions.

Furthermore, the differences in selectivity and hydrocarbon distribution observed for catalysts with similar cobalt sizes suggest the additional effect of the support properties and/or the interaction metal-support. Anderson Schulz Flory (ASF) distribution plots were used for the calculation of the chain growth probabilities for each of the Co-Na-Mo catalyst systems. The results from these calculations are shown in Table 1. The hydrocarbon distribution obtained for all catalysts fits with the ASF equation indicating their formation through the Fischer-Tropsch process<sup>19</sup>, which supports the RWGS-FT tandem mechanism for the reduction of  $\text{CO}_2$  to hydrocarbons. Co-Na-Mo supported on  $\text{TiO}_2$  present the highest chain growth probability and consequently the formation of longer hydrocarbon products. The other inorganic oxide supports present slightly lower chain growth

probability values showing the following trend  $\text{TiO}_2 > \text{CeO}_2 > \text{Al}_2\text{O}_3 > \text{ZrO}_2$ , with methane selectivities in the range of 20 – 30 %. These low methane selectivities compare well with values previously reported for iron based catalysts,<sup>6a</sup> and are significantly lower than previously reported data for cobalt based catalysts.<sup>10,12-13</sup> One should notice that  $\text{Al}_2\text{O}_3$  and  $\text{TiO}_2$  are the most common supports in Fischer-Tropsch applications.<sup>15,20</sup> Interestingly, Co-Na-Mo/ $\text{SiO}_2$  shows relatively high methane selectivity (58%) while ZSM-5 (aluminosilicate) presents the lowest chain probability value with the preferential formation of methane versus longer HC. On the other hand Co-Na-Mo/MgO shows negligible FT activity. Thus, methane selectivity increases as the cobalt particle size decreases, with larger particles (> 20 nm) favouring the formation of long chain hydrocarbons.<sup>21</sup> To demonstrate that the higher methane selectivities presented by the catalysts supported on  $\text{SiO}_2$  and ZSM-5 are not an artefact of the higher  $\text{CO}_2$  conversion achieved with these catalysts, an additional catalytic test was carried out with the Co-Na-Mo/ $\text{SiO}_2$  catalysts where the (weight hourly space velocity) WHSV was adjusted to achieve similar  $\text{CO}_2$  conversion to the one achieved with the catalysts supported on  $\text{Al}_2\text{O}_3$ ,  $\text{CeO}_2$ ,  $\text{TiO}_2$  and ZrO (Entry 2, Table 1). The hydrocarbon distribution appears to be independent of the  $\text{CO}_2$  conversion, with differences within the experimental error.

The interaction of the metal – support can be elucidated by temperature programme reduction (TPR) analysis of the different catalysts (Figure 2). In most of the cases, the TPR profile is complex, with the individual reduction peaks of cobalt and molybdenum overlapping. Additionally, the presence of sodium (as electron donating metal) is also likely to modify the reduction profile of cobalt.<sup>22</sup> Although curve fitting of the peaks is unfeasible due to the close proximities of the peaks, two different main regions can be observed in the TPR profiles corresponding to the hydrogen consumption at temperatures between 250-400 °C and 450-650 °C,

indicated by vertical dashed lines in Figure 2. The first region is attributed to the  $\text{Co}_3\text{O}_4$  reduction into  $\text{CoO}$  and the second one to its further reduction to metallic cobalt.<sup>23</sup> The TPR profile of the supports (without the presence of metals) show negligible hydrogen consumption in comparison to the Co-Na-Mo supported systems except the ceria support which presents a small reduction peak at  $\sim 850$  °C related to the reduction of bulk oxygen and its consequent decomposition.<sup>24</sup> The data in Figure 2 is normalised per mass of catalysts and therefore, differences in the amplitude of the peaks provide information related the degree of reduction of cobalt and molybdenum in the catalysts as well as the interaction with the support, however, it is important to notice that the catalysts are pre-reduced at 300 °C (shadowed area in Figure 2). According to this, it is clear that cobalt is not present in its metallic state under the reaction conditions independently of the support used, however, different degrees of  $\text{Co}_3\text{O}_4$  and  $\text{CoO}$  are present in the catalysts depending on the support used.

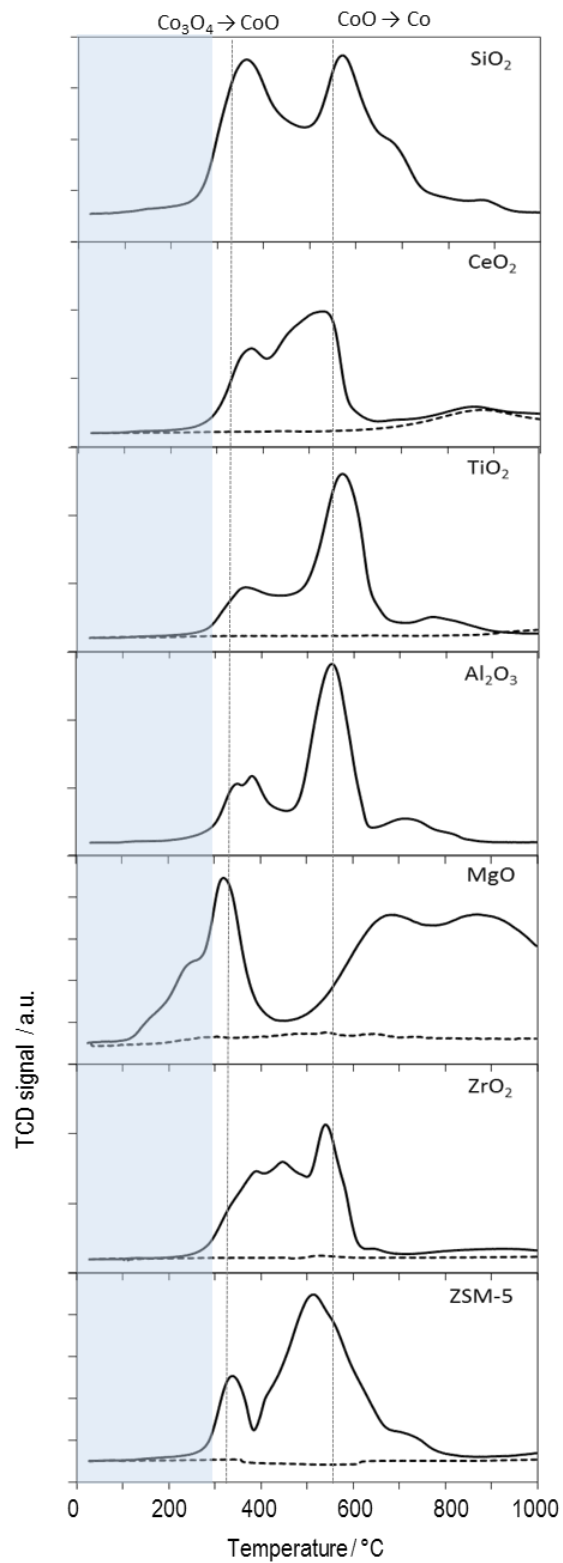


**Figure 2: TPR profiles of the Co-Na-Mo catalysts using different supports. Dashed line corresponds to the TPR of the ceria support. The other supports show negligible hydrogen consumption.**

The small cobalt crystallite particles (< 2 nm) supported on MgO, present also a strong interaction with the support, as evidenced by the highest reduction temperature (> 600 °C). Additionally, this Co-Na-Mo/MgO presents the lowest reduction temperature to CoO, with full reduction of Co<sub>3</sub>O<sub>4</sub> into CoO during the pre-reduction treatment. Most interesting is the fact that the Co-Na-Mo catalysts supported on SiO<sub>2</sub>, CeO<sub>2</sub>, TiO<sub>2</sub>, Al<sub>2</sub>O<sub>3</sub> and ZrO<sub>2</sub> seems to have a stronger metal-support interaction than the counterpart catalyst supported on ZSM-5 as evidenced by their lower reduction temperature to metallic cobalt (at least 40 °C). This metal-support interaction, in conjunction with the cobalt crystallite size, is likely to be responsible for the different hydrocarbon distribution, and the difference in chain growth probability. Thus, for a given cobalt crystallite size, the weaker metal-support interaction, the shorter hydrocarbon chains formed.

Further focus on C<sub>2</sub>-C<sub>4</sub> olefin selectivity of the different Co-Na-Mo catalysts is considered following the currently a renewed interest in the formation of unsaturated short chained (C<sub>2</sub>-C<sub>4</sub>) hydrocarbons,<sup>25</sup> as building blocks for the formation of polymers, detergents and many other chemicals.<sup>26</sup> The Co-Na-Mo catalysts supported on SiO<sub>2</sub> and ZSM-5 show very small selectivity towards unsaturated products, probably to be related to the presence of cobalt crystallite sizes in the order of 14-16 nm as discussed above. Amongst the catalysts with cobalt crystallite sizes between 22-35 nm, the one supported on TiO<sub>2</sub> shows the highest C<sub>2</sub>-C<sub>4</sub> olefin selectivity, with similar olefin selectivity values shown by other reducible oxide supports such as ZrO<sub>2</sub>, CeO<sub>2</sub> and the Al<sub>2</sub>O<sub>3</sub>. In this case, the effect of cobalt particle size seems to be more significant than metal-support interaction for the formation of unsaturated products versus saturated ones.

### 3.2 Mixed SiO<sub>2</sub>:TiO<sub>2</sub> Oxides as Catalyst Supports

Ideally, one will seek a catalytic system with a high CO<sub>2</sub> conversion (as shown by the Co-Na-Mo catalysts supported on SiO<sub>2</sub> and ZSM-5) and a high chain growth probability and olefins selectivity (as shown by Co-Na-Mo supported on TiO<sub>2</sub>). In order to achieve both high conversion and a favourable selectivity, investigations were conducted on mixed TiO<sub>2</sub>:SiO<sub>2</sub> supports to determine whether a synergetic effect could be achieved. The mixed oxide catalyst supports were prepared using a wet kneading method similar to that employed in Jones *et al.*<sup>27</sup> The TiO<sub>2</sub> content on the final material was varied within the 0 to 100% wt.% range, resulting in six mixed-oxide supports; 100 wt.% SiO<sub>2</sub>, 75 wt.% SiO<sub>2</sub> – 25 wt.% TiO<sub>2</sub>, 50 wt.% SiO<sub>2</sub> – 50 wt.% TiO<sub>2</sub>, 25 wt.% SiO<sub>2</sub> – 75 wt.% TiO<sub>2</sub>, 10 wt.% SiO<sub>2</sub> – 90 wt.% TiO<sub>2</sub> and 100 wt.% TiO<sub>2</sub>. SEM and EDX mapping was used to study the morphology and homogeneity of the mixed SiO<sub>2</sub>:TiO<sub>2</sub> supports. Figure 3 shows the data for the 50:50 SiO<sub>2</sub>:TiO<sub>2</sub> system for illustration. It can be observed that a good mixing of the two oxides is achieved. However, elemental mapping shows distinctive regions with high silicon content and regions with high titanium content showing the lack of interaction between the oxides despite the homogeneous composition at a macroscopic level.

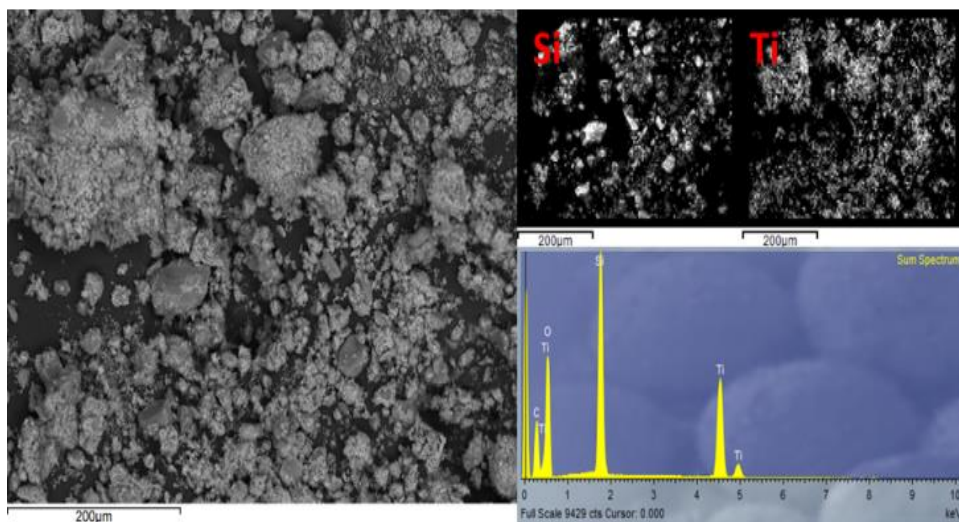
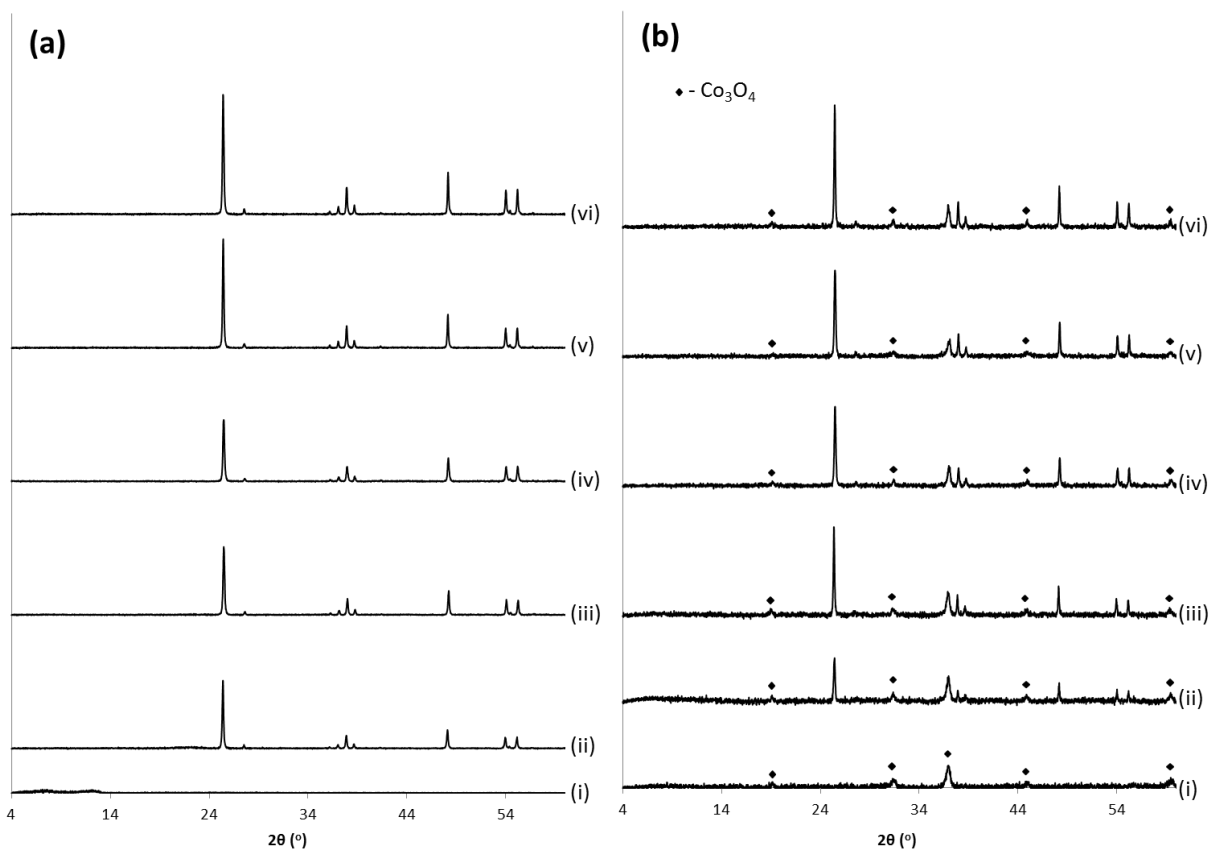


Figure 3: SEM micrograph and EDX mapping for the 50:50 SiO<sub>2</sub>:TiO<sub>2</sub> mixed oxide.

Cobalt, sodium and molybdenum were impregnated following the same procedure as used with the pure oxide supports. The X-ray diffraction patterns before and after metal impregnation are shown in Figure 4 a and b respectively. Pure silica only presents broad diffraction peaks at  $2\theta$  values between 4-14, typical of poorly crystalline  $\text{SiO}_2$ .<sup>28</sup> When titania is added into the system, additional diffraction peaks at  $2\theta$  values of 25, 38, 48 and 55 degrees appear, corresponding to the anatase phase of  $\text{TiO}_2$ .<sup>16a</sup> These diffraction peaks increase in intensity as the titania content increases as expected. The diffraction patterns obtained after impregnation with cobalt, sodium and molybdenum are shown in Figure 4b. No significant change in the peaks attributable to the support oxides was observed indicating that no change in phase or formation of mixed oxides occurred during the calcination step. Additionally, diffraction peaks corresponding to  $\text{Co}_3\text{O}_4$  are observed (marked in the patterns) in all the systems with no evidence of crystalline sodium or molybdenum crystalline phases. In this case and to avoid misleading interpretations, the average cobalt crystalline size is not reported as it provides a simple arithmetic average of the mixed systems with such value not being representative of the real size.



**Figure 4: pXRD patterns of a. mixed SiO<sub>2</sub>-TiO<sub>2</sub> supports and b. their corresponding 20 wt.% Co- 1wt.%Na – 1 wt.% Mo catalysts (i) 100 wt.% SiO<sub>2</sub>, (ii) 75 wt.% SiO<sub>2</sub> – 25 wt.% TiO<sub>2</sub>, (iii) 50 wt.% SiO<sub>2</sub> – 50 wt.% TiO<sub>2</sub>, (iv) 25 wt.% SiO<sub>2</sub> – 75 wt.% TiO<sub>2</sub>, (v) 10 wt.% SiO<sub>2</sub> – 90 wt.% TiO<sub>2</sub> and (vi) 100 wt.% TiO<sub>2</sub> All peaks attributable solely to Co<sub>3</sub>O<sub>4</sub> are marked however, any overlapping with support peaks are not marked for clarity.**

The different catalysts supported on SiO<sub>2</sub>-TiO<sub>2</sub> mixed supports were tested for the direct hydrogenation of CO<sub>2</sub> into hydrocarbons under the same reaction conditions used in order to provide further evidence of the effect of support on the resulting yield. The data obtained from these tests are summarised in Table 3. There is a linear relationship between TiO<sub>2</sub> content in the support and CO<sub>2</sub> conversion as shown in Figure 5a suggesting that a synergetic effect is not achieved in the mixed support systems. A similar conclusion can be drawn from the effect of the mixed TiO<sub>2</sub> – SiO<sub>2</sub> supports on the methane and C<sub>2+</sub> selectivity. The former increases as the TiO<sub>2</sub> content on the support increases, with an opposite effect is observed in the latter. In both cases, the

linear relationship between the selectivity values and the TiO<sub>2</sub> content in the support suggest that a synergetic effect is not achieved in the product distribution and similar values would be obtained if a physical mixture of the Co-Na-Mo/TiO<sub>2</sub> and Co-Na-Mo/SiO<sub>2</sub> is used as a catalyst. However, these data shows that the product distribution can be easily tuned by simply altering the composition of mixed supports.

**Table 3: Catalytic activity of 20wt.%Co-1wt.%Na-1wt.%Mo supported on mixed SiO<sub>2</sub>-TiO<sub>2</sub> oxides..**

Entry	TiO <sub>2</sub> content in mixed SiO <sub>2</sub> -TiO <sub>2</sub> / wt%	CO <sub>2</sub> Conversion /%	CO selectivity /%	HC selectivity /%	Hydrocarbon Distribution							Olefin Selectivity /% <sup>a</sup>
					C <sub>1</sub>	C <sub>2=</sub>	C <sub>2</sub>	C <sub>3=</sub>	C <sub>3</sub>	C <sub>4</sub>	C <sub>5+</sub>	
<b>1</b>	0	30.0	21.5	78.5	57.1	0.0	9.3	0.1	11.8	9.3	12.3	0.7
<b>2</b>	25	24.8	42.9	57.1	53.7	0.0	11.0	0.5	13.6	10.0	11.1	1.9
<b>3</b>	50	26.9	41.2	58.8	40.0	0.0	9.5	0.3	12.8	10.2	27.3	1.5
<b>4</b>	75	18.0	40.0	60.0	31.9	0.0	10.1	1.7	14.8	17.1	24.4	6.5
<b>5</b>	90	13.8	70.8	29.2	32.0	0.0	11.3	5.4	11.7	13.3	26.4	19.1
<b>6</b>	100	13.5	66.7	33.3	23.1	0.8	9.9	9.2	7.0	13.7	24.2	37.3

Reaction conditions 200 °C, 1 atm, 3:1 H<sub>2</sub>:CO<sub>2</sub> and 8 sccm total flow, WHSV: 0.35 h<sup>-1</sup>. <sup>a</sup> Olefin (C<sub>2</sub>-C<sub>4</sub>) content (mol.%).

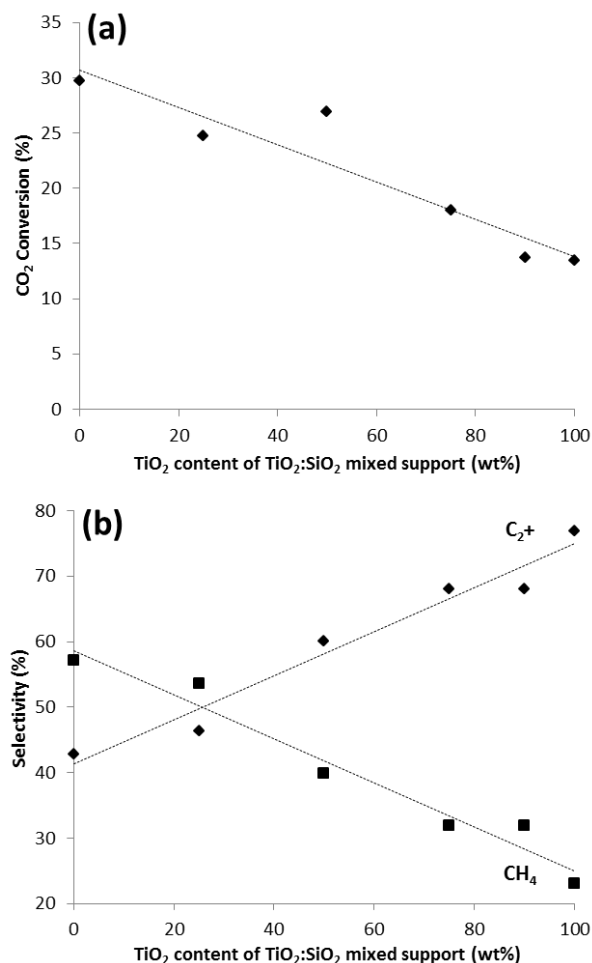


**Figure 5: Relationship between TiO<sub>2</sub> content in the mixed TiO<sub>2</sub>-SiO<sub>2</sub> support and the a. CO<sub>2</sub> conversion and b. CH<sub>4</sub> and C<sub>2+</sub> selectivity in the 20 wt.% Co- 1wt.%Na – 1 wt.% Mo catalysts .**

#### 4. Conclusions

In conclusion a series of Co-Na-Mo catalysts have been prepared and screened for the simultaneous RWGS reaction and FT chemistry. It has been found that systems involving TiO<sub>2</sub> and CeO<sub>2</sub> provide the highest  $\alpha$ -values. These results have been discussed in terms of the cobalt particle size and support interactions. Further, in an attempt to utilise the “best of both worlds” high conversion (SiO<sub>2</sub>) and high selectivity (TiO<sub>2</sub>) mixed systems have been prepared. It can be shown that the conversion/selectivity can be tuned by altering the TiO<sub>2</sub>:SiO<sub>2</sub> ratio in the support.

## 5. Acknowledgements:

We wish to thank the University of Bath for funding this work programme.

## 6. References

† Supporting information available which details further experimental procedures.

- (1) (a) Aresta, M.; Dibenedetto, A.; Angelini, A. *J. CO<sub>2</sub> Utilization* **2013**, 3–4, 65. (b) Centi, G.; Quadrelli, E. A.; Perathoner, S. *Energ. Environ. Sci.* **2013**, 6, 1711. (c) Peters, M.; Köhler, B.; Kuckshinrichs, W.; Leitner, W.; Markewitz, P.; Müller, T. E. *ChemSusChem* **2011**, 4, 1216. (d) Wang, W.; Wang, S.; Ma, X.; Gong, J. *Chem. Soc. Rev.* **2011**, 40, 3703.
- (2) IPCC *Climate Change 2007: Synthesis Report. Contribution of Working Groups I, II and III to the Fourth Assessment Report of the Intergovernmental Panel on Climate Change*; Cambridge University Press, 2007.
- (3) (a) Bothe, H.; Schmitz, O.; Yates, M. G.; Newton, W. E. *Microbiol. Mol. Biol. R.* **2010**, 74, 529. (b) Korpås, M.; Greiner, C. J. *Renew. Energ.* **2008**, 33, 1199. (c) Kudo, A.; Miseki, Y. *Chem. Soc. Rev.* **2009**, 38, 253. (d) Millet, P.; Ngameni, R.; Grigoriev, S. A.; Fateev, V. N. *Int. J. Hydrogen Energ.* **2011**, 36, 4156.
- (4) Centi, G.; Iaquaniello, G.; Perathoner, S. *ChemSusChem* **2011**, 4, 1265.
- (5) (a) Riedel, T.; Claeys, M.; Schulz, H.; Schaub, G.; Nam, S.-S.; Jun, K.-W.; Choi, M.-J.; Kishan, G.; Lee, K.-W. *Appl. Catal. A-Gen.* **1999**, 186, 201. (b) Mattia, D.; Jones, M.D.; O'Byrne, J.P.; Griffiths, O.G.; Owen, R.E.; Sackville, E.; McMannus, M.; Plucinski, P.; *ChemSusChem*, **2015**, 8, 4064.
- (6) (a) Saeidi, S.; Amin, N. A. S.; Rahimpour, M. R. *J. CO<sub>2</sub> Utilization* **2014**, 5, 66. (b) Sai Prasad, P. S.; Bae, J.; Jun, K.-W.; Lee, K.-W. *Catal. Surv. Asia* **2008**, 12, 170. (c) Dorner, R. W.; Hardy, D. R.; Williams, F. W.; Willauer, H. D. *Energ. Environ. Sci.* **2010**, 3, 884. (d) Torrente-Murciano, L.; Chapman, R.S.L.; Narvaez-Dinamarca, A.; Mattia, D.; Jones, M.D. *Phys. Chem. Chem. Phys.*, 2016, DOI: 10.1039/C5CP07788E
- (7) (a) Dry, M. E. *Catal. Today* **2002**, 71, 227. (b) Schulz, H. *Appl. Catal. A Gen.*, **1999**, 186, 3.
- (8) Riedel, T.; Schaub, G.; Jun, K.-W.; Lee, K.-W. *Ind. Eng. Chem. Res.*, **2001**, 40, 1355.
- (9) Visconti, C. G.; Lietti, L.; Tronconi, E.; Forzatti, P.; Zennaro, R.; Finocchio, E. *Appl. Catal. A-Gen.* **2009**, 355, 61.
- (10) Dorner, R. W.; Hardy, D. R.; Williams, F. W.; Davis, B. H.; Willauer, H. D. *Energ. Fuel* **2009**, 23, 4190.
- (11) Bukur, D. B.; Mukesh, D.; Patel, S. A. *Ind. Eng. Chem. Res.* **1990**, 29, 194.
- (12) Zhang, Y.; Jacobs, G.; Sparks, D. E.; Dry, M. E.; Davis, B. H. *Catal. Today* **2002**, 71, 411.
- (13) Owen, R. E.; O'Byrne, J. P.; Mattia, D.; Plucinski, P.; Pascu, S. I.; Jones, M. D. *Chem. Commun.* **2013**, 49, 11683.
- (14) Jacobs, G.; Das, T. K.; Zhang, Y.; Li, J.; Racoillet, G.; Davis, B. H. *Appl. Catal. A-Gen* **2002**, 233, 263.
- (15) Reuel, R. C.; Bartholomew, C. H. *J. Catal.* **1984**, 85, 78.
- (16) (a) Sun, C. H.; Yang, X. H.; Chen, J. S.; Li, Z.; Lou, X. W.; Li, C.; Smith, S. C.; Lu, G. Q.; Yang, H. G. *Chem. Commun.* **2010**, 46, 6129. (b) Taguchi, M.; Takami, S.; Adschiri, T.; Nakane, T.; Sato, K.; Naka, T. *CrystEngComm* **2011**, 13, 2841. (c) Niu, H.; Yang, Q.;

- Tang, K.; Xie, Y. *Scripta Mater.* **2006**, *54*, 1791. (d) Sherafat, Z.; Antunes, I.; Almeida, C.; Frade, J. R.; Paydar, M. H.; Mather, G. C.; Fagg, D. P. *Dalton Trans.* **2014**, *43*, 9324.
- (17) Wang, Y.-Z.; Zhao, Y.-X.; Gao, C.-G.; Liu, D.-S. *Catal. Lett.* **2008**, *125*, 134.
- (18) Torrente-Murciano, L.; Lapkin, A. A.; Chadwick, D. *J. Mater. Chem.* **2010**, *20*, 6484.
- (19) Fujiwara, M.; Ando, H.; Matsumoto, M.; Matsumura, Y.; Tanaka, M.; Souma, Y. *Chem. Letts* **1995**, *24*, 839.
- (20) Iglesia, E.; Soled, S. L.; Fiato, R. A. *J. Catal.* **1992**, *137*, 212.
- (21) (a) den Breejen, J. P.; Radstake, P. B.; Bezemer, G. L.; Bitter, J. H.; Frøseth, V.; Holmen, A.; de Jong, K. P. *J. Am. Chem. Soc.* **2009**, *131*, 7197. (b) Khodakov, A. Y.; Griboval-Constant, A.; Bechara, R.; Zholobenko, V. L. *J. Catal.* **2002**, *206*, 230.
- (22) Hill, A. K.; Torrente-Murciano, L. *Int. J. Hydrog. Energy* **2014**, *39*, 7646.
- (23) Fischer, N.; van Steen, E.; Claeys, M. *Catal. Today* **2011**, *171*, 174.
- (24) Torrente-Murciano, L.; Gilbank, A.; Puertolas, B.; Garcia, T.; Solsona, B.; Chadwick, D. *Appl. Catal. B-Environ.* **2013**, *132–133*, 116.
- (25) Torres Galvis, H. M.; Bitter, J. H.; Khare, C. B.; Ruitenbeek, M.; Dugulan, A. I.; de Jong, K. P. *Science* **2012**, *335*, 835.
- (26) Hu, B.; Frueh, S.; Garces, H. F.; Zhang, L.; Aindow, M.; Brooks, C.; Kreidler, E.; Suib, S. L. *Appl. Catal. B-Environ.* **2013**, *132–133*, 54.
- (27) Lewandowski, M.; Babu, G. S.; Vezzoli, M.; Jones, M. D.; Owen, R. E.; Mattia, D.; Plucinski, P.; Mikolajska, E.; Ochendusko, A.; Apperley, D. C. *Catal. Commun.* **2014**, *49*, 25.
- (28) Kim, M.-Y.; Choi, J.-S.; Toops, T.; Jeong, E.-S.; Han, S.-W.; Schwartz, V.; Chen, J. *Catalysts* **2013**, *3*, 88.